Vortex stability in nearly-two-dimensional Bose-Einstein condensates with attraction

Dumitru Mihalache,[1,2] Dumitru Mazilu,[1,2] Boris A. Malomed,[3] and Falk Lederer[1]
[1]*Institute of Solid State Theory and Theoretical Optics, Friedrich-Schiller Universität Jena, Max-Wien-Platz 1, D-077743 Jena, Germany*
[2]*National Institute of Physics and Nuclear Engineering, Department of Theoretical Physics, Institute of Atomic Physics, P.O. Box MG-6, Bucharest, Romania*
[3]*Department of Interdisciplinary Studies, Faculty of Engineering, Tel Aviv University, Tel Aviv 69978, Israel*
(Received 28 July 2005; published 26 April 2006)

We perform accurate investigation of stability of localized vortices in an effectively two-dimensional ("pancake-shaped") trapped Bose-Einstein condensate with negative scattering length. The analysis combines computation of the stability eigenvalues and direct simulations. The states with vorticity $S=1$ are stable in a third of their existence region, $0<N<(1/3)N_{\max}^{(S=1)}$, where N is the number of atoms, and $N_{\max}^{(S=1)}$ is the corresponding collapse threshold. Stable vortices easily self-trap from arbitrary initial configurations with embedded vorticity. In an adjacent interval, $(1/3)N_{\max}^{(S=1)}<N<0.43N_{\max}^{(S=1)}$, the unstable vortex periodically splits in two fragments and recombines. At $N>0.43N_{\max}^{(S=1)}$, the fragments do not recombine, as each one collapses by itself. The results are compared with those in the full three-dimensional (3D) Gross-Pitaevskii equation. In a moderately anisotropic 3D configuration, with the aspect ratio $\sqrt{10}$, the stability interval of the $S=1$ vortices occupies $\approx 40\%$ of their existence region, hence the two-dimensional (2D) limit provides for a reasonable approximation in this case. For the isotropic 3D configuration, the stability interval expands to 65% of the existence domain. Overall, the vorticity heightens the actual collapse threshold by a factor of up to 2. All vortices with $S\geqslant 2$ are unstable.

DOI: 10.1103/PhysRevA.73.043615 PACS number(s): 03.75.Lm, 03.65.Ge, 05.45.Yv

I. INTRODUCTION

Vortices are fundamental dynamical objects in Bose-Einstein condensates (BECs) [1]. They can be easily created in large numbers, forming vortex lattices [2]. A review of basic results for the BEC vortices can be found in Ref. [3]. In most works, vortices were studied in self-repulsive BECs, with a positive scattering length characterizing collisions between atoms. In the experiment, vortices are created stirring the condensate by a properly designed laser beam [1], or by imprinting an appropriate phase pattern onto a condensate trapped in a Joffe-Pritchard magnetic trap [4]. Recently, more complex vortical structures were predicted in repulsive condensates, such as vortex dipoles [5] and quadrupoles [6], and patterns in the form of globally linked topological defects [7].

Vortices in repulsive BECs may be regarded as dark solitons on a finite background, similar to optical vortices in a self-defocusing dielectric medium [8]. A challenging issue is the study of *vortex solitons* (completely localized objects with embedded vorticity) in attractive BECs, with a negative scattering length [9]. In particular, attractive interaction occurs in the ^{7}Li condensate [10], where quasi-one-dimensional solitons were created [11].

The most natural setting for vortex solitons is a "pancake" condensate, strongly confined in one direction (z) and weakly trapped in the radial direction (r) in the transverse plane. In the experiment, the "pancake" is created by a superposition of a tight optical trap, with a confinement thickness a_z, and a loose radial magnetic trap with a trapping frequency Ω_r in the transverse plane [12]. The theoretical description of the "pancake" configuration assumes that the underlying three-dimensional (3D) Gross-Pitaevskii equation (GPE) may be reduced to its 2D counterpart. The condition necessary for the reduction is that the squared harmonic-oscillator length determined by the radial trapping frequency Ω_r,

$$(a_r^{(\mathrm{ho})})^2 = \hbar/(m\Omega_r) \tag{1}$$

(m is the atomic mass), must be much larger than a_z^2, i.e.,

$$\Omega_r \ll \pi^2 \hbar/(ma_z^2). \tag{2}$$

For Li atoms trapped in the diffraction-limited gap between two parallel strongly repulsive (blue-detuned) light sheets, with $a_z \simeq 2$ μm, this means $\Omega_r \ll 10$ kHz, which is readily met in the experiment, where confining frequencies are measured in tens of Hz. Condition (2) also rule out bending instability of vortex cores in the pancake geometry (in the full 3D case, the instability results in decay of straight vortices into vortex rings, in repulsive condensates [13]), as a_z is much smaller than the vertical length necessary for the bending.

The condition (2) for the applicability of the 2D approximation can be cast in another form, which sets a limit on the number of atoms $\mathcal{N}$ in the pancake-shaped condensate. As shown below, this form is

$$\mathcal{N} \lesssim \frac{\hbar}{m\Omega_r |a| a_z}, \tag{3}$$

where a is the (negative) scattering length. Taking the same value $a_z=2$ μm as above, together with experimentally relevant $\Omega_r=10$ Hz [in this case, Eq. (1) yields $a_r^{(\mathrm{ho})} \simeq 10$ μm for Li atoms], and $a=-0.1$ nm, which is typical for soliton experiments in ^{7}Li [10,11], Eq. (3) yields $\mathcal{N} \lesssim 10^4$.

Generally, vortex solitons are unstable against collapse (catastrophic self-compression of the wave function), and also against azimuthal perturbations which break the axial symmetry of the solitons. In fact, condition (3) provides for the stability of the quasi-2D solitons against the 3D collapse. Within the framework of the 2D description, both the ordinary (zero-vorticity) solitons and their vortical counterparts can be stabilized by a square-shaped optical lattice (OL) [14,15]. The same OL can also support weakly localized vortex solitons of the *gap type* in a repulsive BEC [16,17]; a quasi-1D lattice stabilizes ordinary solitons, but not vortices, in the 2D model with self-attraction [16,18]. In attractive condensates, ordinary 3D solitons can be stabilized by low-dimensional OLs (viz., a quasi-2D lattice [16,18,19]), or an axially symmetric one [20]), as well as by the full 3D lattice [21] (for a recent review of multidimensional solitons in optics and BEC, see Ref. [22]). In addition, 2D zero-vorticity solitons can be stabilized by means of the *Feshbach-resonance management* [23], which amounts to time-periodic modulation of the scattering length between positive and negative values [24]. However, the latter mechanism cannot stabilize vortex solitons [25], although it may inhibit the development of their instability [26].

While vortex solitons of the 2D GPE with a negative scattering length are strongly unstable in free space, they can be stabilized by the radial trapping potential, $(m/2)\Omega_r^2 r^2$. This issue was considered in an early work [27] and more recently [28,29]. It is well known that the radial trap stabilizes zero-vorticity ($S=0$) states against collapse, provided that the norm of the solution (which is proportional to the number of atoms in the condensate) is limited from above. In the 3D case with the isotropic radial trap, the maximum norm depends on the corresponding trapping frequency Ω_r. This maximum norm was found by means of the variational approximation and from numerical computations [27,28]. In contrast to that, the maximum 2D norm, $N_{\max}^{(S=0)}$, *does not* depend on Ω_r, being exactly equal to the norm of the corresponding *Townes soliton* in the free 2D space [30]. Similarly, the maximum value of the norm for the trapped fundamental vortex (one with $S=1$), which does not lead to collapse, depends on Ω_r in the 3D case (the shape of the 3D trap which maximizes the collapse threshold under additional conditions was studied in Ref. [31]), but not in the 2D situation, where it coincides with the known collapse threshold, $N_{\max}^{(S=1)}$, of the fundamental vortex soliton in free space [32]. Formally, the vorticity gives rise to a dramatic increase of the 2D collapse threshold, $N_{\max}^{(S=1)} \approx 4N_{\max}^{(S=0)}$. However, we will demonstrate that the actual increase of the 2D stability threshold, $N_{\rm thr}$, in the fundamental vortex is a more modest effect, amounting to $N_{\rm thr} \simeq 2N_{\max}^{(S=0)}$; in the remaining part of the existence interval for the vortex, $N_{\rm thr} < N < N_{\max}^{(S=1)}$, the azimuthal instability splits the vortex into a pair of fragments, which then collapse intrinsically.

It is relevant to mention that, in various models of nonlinear optics (see Refs. [33] and brief reviews [34]), vortex solitons, while being stable against radial perturbations, are easily split into fragments by an azimuthal instability. Nevertheless, *azimuthally stable* vortical solitons have been predicted too, in models with competing [35] or nonlocal nonlinearities [36], and in defocusing media with an imprinted cylindrical lattice [37].

In this work, we aim to investigate the stability of vortices in the 2D GPE equation with self-attraction and weak radial trapping potential, through computation of a full set of the corresponding stability eigenvalues. The results will be verified by direct simulations. We conclude that all vortices with $S \geqslant 2$ are unstable (as conjectured in Ref. [28]), while the fundamental ones ($S=1$) are completely stable for $0 < N < N_{\rm cr} \approx (1/3)N_{\max}^{(S=1)}$ [in Ref. [28], it was conjectured that $N_{\rm cr} \simeq (1/4)N_{\max}^{(S=1)}$]. At $N=N_{\rm cr}$, the $S=1$ vortex is destabilized by symmetry-breaking oscillatory perturbations. Further, in an adjacent interval, $(1/3)N_{\max}^{(S=1)} < N < 0.43N_{\max}^{(S=1)}$, the evolution of the unstable vortex *does not* lead to collapse; instead, it features nearly periodic splittings in two fragments followed by their recombinations back into the vortex. This regular dynamical regime was not known before. In the remaining part of the existence interval, $0.43N_{\max}^{(S=1)} < N < N_{\max}^{(S=1)}$, fragments produced by the splitting of the vortex do not recombine, but rather blow up intrinsically, as their individual norm exceeds the collapse threshold for the Townes soliton.

We will also verify that the results obtained within the framework of the 2D model are valid indeed in the full 3D GPE with the corresponding anisotropic trap. In particular, in a moderately anisotropic 3D model, with the radial-confinement length $a_r^{(\rm ho)}$ [see Eq. (1)] larger by a factor of $\sqrt{10}$ than its counterpart, $a_z^{(\rm ho)}$, in the orthogonal (tightly confined) direction, the relative size of the stability area inside the existence region for 3D solitons with the embedded vorticity $S=1$ is ≈ 0.4, which is to be compared to the above-mentioned relative size of the stability region, 1/3, in the 2D limit. Approaching the isotropic limit, $a_z^{(\rm ho)}/a_r^{(\rm ho)} \to 1$, the stability area expands, attaining the relative size ≈ 0.65.

The paper is organized as follows. In Sec. II, we formulate the 2D model, briefly recapitulating its derivation from the 3D GPE. In Sec. III, we present basic results for the 2D model: shapes of the vortex states (actually, we find them by continuation of exact states with a definite value of the angular momentum in the linear 2D Schrödinger equation), and eigenvalues that determine their stability. In Sec. IV, we verify the predicted stability conditions by direct simulations. In Sec. V, we consider the full 3D model with the anisotropic trap, and Sec. V concludes the paper.

II. THE MODEL

We assume a self-attractive condensate which is loaded in a nonrotating loose trap in the (x,y) plane, and tightly confined in the z direction. The corresponding 3D GPE for the single-atom wave function Ψ is [38]

$$i\hbar \frac{\partial \Psi}{\partial t} = \left(-\frac{\hbar^2}{2m}\nabla^2 + \frac{m}{2}[\Omega_r^2(x^2+y^2) + \Omega_z^2 z^2] + \frac{4\pi\hbar^2 a}{m}|\Psi|^2 \right)\Psi, \tag{4}$$

where ∇^2 is the 3D Laplacian and a is the negative

s-scattering length accounting for the attraction between atoms. In the pancake configuration, the confinement frequency Ω_z is assumed to be much larger than Ω_r. If the tight confinement in the z direction is provided by parallel light sheets repelling the atoms, the corresponding potential term, instead of $m\Omega_z^2 z^2/2$, is a deep rectangular potential well in the region of $0<z<a_z$.

The 3D equation can be reduced to an effective GPE in two dimensions, provided that the transverse quantum pressure is much stronger than self-attraction. In other words, the energy of the atom in the ground state of the vertical trap, if the latter is taken as the deep potential well of width a_z,

$$E_0 = (\pi\hbar)^2/(2ma_z^2), \tag{5}$$

must be much larger than the contribution of the attraction to the atomic chemical potential, $\Delta\mu \sim -2\pi\hbar^2(a/m)n$, where $n \equiv |\Psi|^2$ is the 3D atom density [if the tight vertical confinement is provided by large Ω_z in Eq. (4), then the respective harmonic-oscillator length, $a_z^{(\mathrm{ho})} = \sqrt{\hbar/(m\Omega_z)}$, taken as per Eq. (1), defines the effective confinement size as $a_z = \pi a_z^{(\mathrm{ho})}$].

For the pancake-shaped configuration in the weak radial trap, the density is determined, together with a characteristic radial size R of the pancake itself, by the condition of the balance between the radial quantum pressure, radial trapping force, and nonlinear selfattraction, which yields

$$R \sim \sqrt{\frac{\hbar}{m\Omega_r}} \equiv a_r^{(\mathrm{ho})}, \quad n \sim \frac{m\Omega_r}{8\pi a\hbar}. \tag{6}$$

The substitution of expressions (5) and (6) in the above condition $E_0 \gg |\Delta\mu|$, which implies the tight transverse confinement, leads to Eq. (2) that determines the range of the radial trapping frequencies where the 2D description is applicable. As a consequence of this condition, the aspect ratio of the pancake configuration is always large, $\pi R/a_z \sim a_z^{-1}\sqrt{\hbar/(m\Omega_r)} \gg 1$. A limitation on the number of atoms in the pancake state can be derived by noting that it is determined by the product of the density, as given by Eq. (6), and the effective volume, $\simeq \pi R^2 a_z$, which leads to Eq. (3). If $\mathcal{N}$ exceeds this limit, the condensate will start a nearly-2D collapse, which may later go over into a stronger collapse in three dimensions.

The final derivation of the effective 2D equation follows a well-known route: the 3D wave function is factorized,

$$\Psi(x,y,z,t) = \psi(x,y,t)\phi_0(z), \tag{7}$$

where $\phi_0 = \sin(\pi z/a_z)$ is the ground-state wave function of the transverse state between two hard walls separated by the distance a_z. After that, averaging of the 3D equation (4) in the z direction leads to a normalized two-dimensional GPE [39],

$$i\frac{\partial\psi}{\partial t} = \left[-\frac{1}{2}\left(\frac{\partial^2}{\partial x^2} + \frac{\partial^2}{\partial y^2}\right) + \frac{1}{2}\Omega_r^2(x^2+y^2) + g|\psi|^2\right]\psi, \tag{8}$$

where $g \equiv 3\pi a$ (or $g \equiv 2\sqrt{2}\pi a$ for the case of the parabolic trap in the vertical direction), the transverse-ground-state energy E_0 was subtracted from the chemical potential, while Ω_r and t actually stand for $m\Omega_r/\hbar$ and $(\hbar/m)t$. The variables x, y and $|\psi|^2$ in Eq. (8) are measured in the same units as in Eq. (4). We then redefine them too, by $\psi \to \sqrt{|g|/\Omega_r}\psi$, $(x,y) \to \sqrt{\Omega_r}(x,y)$, and additionally rescale time by $t \to \Omega_r t$, to finally set $\Omega_r = -g \equiv 1$ (unless $g=0$).

Equation (8) conserves the 2D norm, $N = \int\int |\psi(x,y,t)|^2 dxdy$, and energy

$$E = \int\int \left[\frac{1}{2}\left(\left|\frac{\partial\psi}{\partial x}\right|^2 + \left|\frac{\partial\psi}{\partial y}\right|^2\right) - \frac{1}{2}g|\psi|^4 + \frac{1}{2}\Omega_r^2(x^2+y^2)|\psi|^2\right]dxdy. \tag{9}$$

A straightforward consequence of Eq. (8) is the relationship $E = \mu N + \pi|g|\int_0^\infty rR^4 dr$, which is used to cross-check the accuracy of numerical results, see below. Further, the above rescalings and factorization (7) result in the following relation between the 2D norm and the number of atoms, $\mathcal{N}$ (which is defined as the norm of the 3D wave function in original units),

$$\mathcal{N} = \frac{a_z}{2|g|}N \equiv \frac{a_z}{6\pi|a|}N, \tag{10}$$

where the second equality follows from the above relation $g = 3\pi a$, if the vertical confinement is provided by the repelling light sheets. If, instead, a tight parabolic potential is used to confine the condensate in the z direction, the coefficient in front of the last term in Eq. (10) is replaced by $a_z^{(\mathrm{ho})}/(2\sqrt{2}|a|)$, where $a_z^{(\mathrm{ho})}$ is the respective linear-oscillator length as defined above.

The final normalized form of the 3D GPE, which is also considered below, is

$$i\frac{\partial\Psi}{\partial t} = \left[-\frac{1}{2}\left(\frac{\partial^2}{\partial x^2} + \frac{\partial^2}{\partial y^2} + \frac{\partial^2}{\partial z^2}\right) + \frac{1}{2}(x^2+y^2+\Omega^2 z^2) - |\Psi|^2\right]\Psi. \tag{11}$$

Here the nonlinearity coefficient is again scaled to be -1, and $\Omega^2 \equiv \Omega_z^2/\Omega_r^2$ measures the relative strength of the tight confinement in the vertical direction, the nearly 2D case corresponding to $\Omega^2 \gg 1$. The norm of the 3D solutions, $N = \int\int\int |\Psi(x,y,z,t)|^2 dxdydz$, is related to the number of atoms as follows:

$$\mathcal{N} = \sqrt{\frac{\hbar}{m\Omega_r}}\frac{N}{8\pi|a|} \equiv \frac{a_r^{(\mathrm{ho})}}{8\pi|a|}N, \tag{12}$$

where $a_r^{(\mathrm{ho})}$ is the harmonic-oscillator length in the radial direction, defined as per Eq. (6). The conserved energy of the 3D condensate is

$$E = \int\int\int \left[\frac{1}{2}\left(\left|\frac{\partial\Psi}{\partial x}\right|^2 + \left|\frac{\partial\Psi}{\partial y}\right|^2 + \left|\frac{\partial\Psi}{\partial z}\right|^2\right) - \frac{1}{2}|\Psi|^4 + \frac{1}{2}(x^2+y^2+\Omega^2 z^2)|\Psi|^2\right]dxdydz. \tag{13}$$

Note that, after Ω_r and $-g$ were normalized to be 1, the two-dimensional GPE (8) features no free parameters, while

its 3D counterpart, Eq. (11), contains one free coefficient, Ω^2.

III. TWO-DIMENSIONAL VORTEX SOLUTIONS AND THEIR LINEAR STABILITY

Stationary vortex solutions to Eq. (8) are looked for as

$$\psi = R(r)\exp(iS\theta - i\mu t), \tag{14}$$

with an integer vorticity S, real chemical potential μ, and function $R(r)$ obeying the equation

$$R'' + r^{-1}R' + (2\mu - S^2r^{-2} - r^2)R - 2gR^3 = 0, \tag{15}$$

where the prime stands for d/dr. In the linear case, $g=0$, Eq. (15) is tantamount to the usual stationary quantum-mechanical Schrödinger equation for the 2D harmonic oscillator, which gives rise to an infinite set of discrete eigenvalues, $\mu=j+k+1$, with $j,k=0,1,2,\ldots$.

In the Cartesian coordinates, the corresponding eigenfunctions are (recall we have set $\Omega\equiv 1$)

$$\psi_{jk}(x,y,t) = e^{-i(j+k+1)t}\Phi_j(x)\Phi_k(y), \tag{16}$$

where $\Phi_j(x)$ and $\Phi_k(x)$ are stationary wave functions of the 1D harmonic oscillator associated with the energy eigenvalues $j+1/2$ and $k+1/2$, respectively. The set of states (16) is degenerate, as all the states corresponding to a fixed value of $j+k$ appertain to the same eigenvalue. Making use of this degeneracy, the eigenfunctions may be rearranged into combinations with a definite value of the vorticity, which is

$$S = j + k \equiv \mu - 1. \tag{17}$$

In particular, the combination

$$\psi_0^{(S=1)} \equiv \psi_{10}(x,y,t) + i\psi_{01}(x,y,t) \equiv r\exp(-2it + i\theta - r^2/2) \tag{18}$$

is the wave function with the lowest value of the chemical potential for $S=1$, $\mu\equiv j+k+1=2$, and

$$\psi_0^{(S=2)} \equiv \psi_{20}(x,y,t) - \psi_{02}(x,y,t) + 2i\psi_{11}(x,y,t) \equiv r^2\exp(-3it + 2i\theta - r^2/2) \tag{19}$$

is the wave function with the lowest chemical potential, $\mu \equiv j+k+1=3$, for $S=2$.

Nonlinear solutions for vortices can be obtained by a continuation method, starting at $g=0$ with expressions (18) and (19). Note that, pursuant to Eq. (15), the shift of μ due to the self-attractive nonlinearity (with $g<0$) is negative, hence from the comparison with the linear result (17) it follows that

$$\mu(N \neq 0) < \mu(N=0) \equiv \mu_{\max} = S + 1. \tag{20}$$

To specify solutions to Eq. (15) in the nonlinear case (recall we set $g=-1$), Eq. (15) was solved numerically. The dependences $\mu(N)$ obtained from the numerical solutions for $S=0,1$ and 2 are plotted in Fig. 1(a) (in a part, these dependences are tantamount to those reported earlier in Ref. [28]). Naturally, μ approaches the linear value $\mu_{\max}$ for $N\to 0$, see Eq. (20), while for large negative μ the norm of the $S=0$ state asymptotically approaches the value $N_{\max}^{(S=0)} \approx 5.85$, which is the above-mentioned collapse threshold corresponding to the Townes soliton [30]. Similarly, for the states with $S\geqslant 1$ the asymptotic values $N(\mu=-\infty)$ are the above-mentioned ones, $N_{\max}^{(S)}$, which determine the (formal) collapse threshold for the vortices.

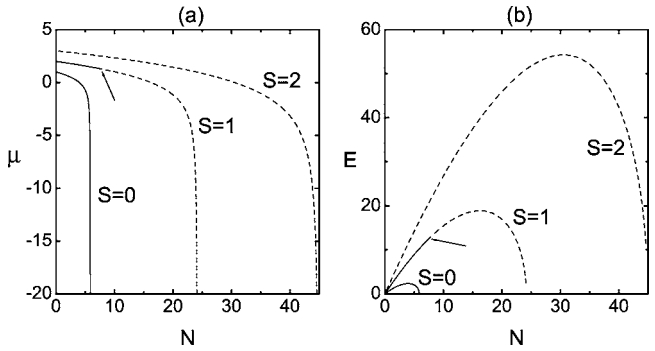

FIG. 1. Chemical potential μ (a) and energy E (b) versus normalized number of atoms N for solutions with vorticities $S=0,1$, and 2, as found from Eq. (15) with $g\equiv -1$. Solid and dashed lines show stable and unstable branches of the solutions (see below). The arrow indicates the point where the $S=1$ vortices loose their stability.

To study stability of the stationary solutions, we search for a perturbed solution of Eq. (8) as

$$\psi(x,y,t) = [R(r) + u(r)\exp(\lambda t + iL\theta) + v^*(r)\exp(\lambda^* t - iL\theta)]\exp(iS\theta - i\mu t), \tag{21}$$

where (u,v) and λ are eigenmodes and the instability growth rate corresponding to an integer azimuthal index L of the perturbation. The linearization around the stationary solution leads to equations

$$i\lambda u + \tfrac{1}{2}[u'' + r^{-1}u' - (S+L)^2r^{-2}u] + \mu u + R^2(v+2u) - \tfrac{1}{2}r^2u = 0,$$

$$-i\lambda v + \tfrac{1}{2}[v'' + r^{-1}v' - (S-L)^2r^{-2}v] + \mu v + R^2(u+2v) - \tfrac{1}{2}r^2v = 0, \tag{22}$$

which were solved numerically, with boundary conditions demanding that $u(r)$ and $v(r)$ decay exponentially at $r\to\infty$, and decay as $r^{|S\pm L|}$ at $r\to 0$.

The most important result following from the numerical computation of eigenvalues λ is that the vortex soliton with $S=1$ is stable, i.e., real parts of all the eigenvalues remain equal to zero, only in a *finite interval* of values of the chemical potential adjacent to the linear limit [see Eq. (20)], $\mu_{\max}(S=1)\equiv 2>\mu>\mu_{\rm cr}\approx 1.276$, and outside this interval, i.e., for $-\infty<\mu<\mu_{\rm cr}$, the states with $S=1$ are unstable. At the critical point ($\mu=\mu_{\rm cr}$), the corresponding critical norm is $N_{\rm cr}^{(2D)}=7.79$. Thus, the vortices with $S=1$ are stable in the region

$$0 \leqslant N < N_{\rm cr}^{(2D)} = 7.79, \tag{23}$$

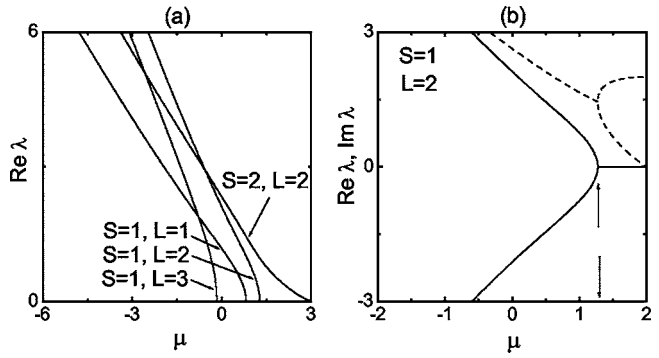

FIG. 2. (a) The real part of the perturbation growth rate λ for different azimuthal indices L. (b) The real and imaginary parts (solid and dashed lines, respectively) of the eigenvalues responsible for the *Hamiltonian-Hopf* bifurcation which destabilizes the vortices with $S=1$ at the critical point, $\mu=\mu_{\rm cr}\approx 1.276$. This value and the bifurcation point are marked by arrows.

and in the remaining *two-thirds* of their existence interval, i.e.,

$$7.79 < N < N_{\rm max}^{(S=1)} \approx 24.1, \tag{24}$$

they are *unstable*. The conclusion that "less nonlinear" solutions, i.e., ones with smaller N, are more stable is quite natural, as they continue the stable linear solutions which correspond to $N=0$ [40].

The energy [see Eq. (9)] at $\mu=\mu_{\rm cr}$ is $E_{\rm cr}=12.913$. The energy as a function of N is displayed, for the $S=1$ soliton family, in Fig. 1(b). It is noteworthy that, while the $\mu(N)$ dependence in Fig. 1(a) is monotonic, its $E(N)$ counterpart is not.

To further characterize the (in)stability of the vortices with $S=1$ and 2, in Fig. 2(a) we show the largest real part of the eigenvalues $\lambda_L^{(S)}$ as a function of μ for different values of the perturbation azimuthal index L, see Eq. (21). Extensive numerical calculations demonstrate that the perturbation mode that actually determines the stability border always has $L=2$. In particular, $\mathrm{Re}(\lambda_{L=2}^{(S=2)})$ is positive in the entire existence domain of the $S=2$ vortices, up to the linear limit, $\mu_{\rm max}(S=2)=3$ [see Eq. (20)], thus making the vortices with $S=2$ *completely unstable* and confirming a conjecture put forward in Ref. [28]. All vortices with $S>2$ are unstable too.

For the fundamental vortex solitons with $S=1$, the numerical calculation of the eigenvalues $\lambda_L^{(S=1)}$ was performed for values of the azimuthal index up to $L=6$, in a broad range of values of the soliton's chemical potential, $-20<\mu<2$. It was found that the maximum value of $\mathrm{Re}(\lambda_L^{(S=1)})$ is nonzero for $L=1,2,3$, and this value is zero (up to the numerical accuracy) for higher values of the azimuthal index, $L=4,5$, and 6. To further check the accuracy of the numerical results, we have compared the eigenvalues produced by the numerical code running on 400 and 800 discretization points, respectively, and concluded that four significant digits are identical in both cases.

The bifurcation responsible for the destabilization of the $S=1$ vortex at $\mu=\mu_{\rm cr}$ is identified by results displayed in Fig. 2(b). As seen from the figure, the bifurcation is of the *Hamiltonian-Hopf* type [41], i.e., it is accounted for by a quartet of complex eigenvalues, $(\lambda,\lambda^*,-\lambda,-\lambda^*)$, cf. earlier reported results for solitons in scalar [42,43] and vectorial [44,45] models. The unstable quartet is generated by a collision of two pairs of imaginary (stable) eigenvalues, which is typical to the Hamiltonian-Hopf bifurcation.

IV. DIRECT SIMULATIONS OF TWO-DIMENSIONAL STABLE AND UNSTABLE VORTICES

To verify the above predictions concerning the stability of the vortex solitons in the 2D approximation, we have performed direct simulations of the perturbed evolution of vortex solitons in Eq. (8). The simulations were carried out by means of the Crank-Nicholson discretization scheme. The system of the corresponding nonlinear finite-difference equations was first solved by means of the Picard iteration method [46], and the resulting linear system was then handled using the Gauss-Seidel iterative scheme. For good convergence we typically needed five Picard iterations and eight Gauss-Seidel iterations. We employed a grid with 600 $\times$600 points (typical stepsizes were $\Delta x=\Delta y=0.025$ and $\Delta t=0.0008$).

To test the stability of the $S=1$ vortex, random noise was added to it at the initial moment – typically, with a 5% relative amplitude. Figure 3 shows how a vortex with $S=1$, that was predicted above to be stable against small perturbations, completely recovers after the addition of the initial perturbations.

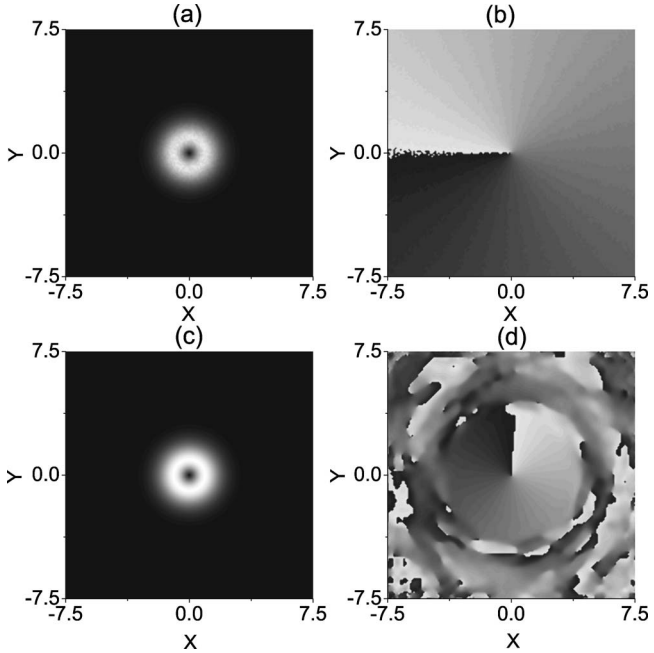

FIG. 3. Grey-scale plots illustrating recovery of the perturbed stable vortex with $S=1$ for $\mu=1.4$. (a),(b) Intensity and phase distributions in the initial configuration including random noise. (c),(d) The same in the self-cleaned vortex soliton at $t=120$. The norms of the input and output solitons are $N=6.641$ and $N=6.629$, respectively (the small loss of the norm is due to absorbers placed at borders of the integration domain).

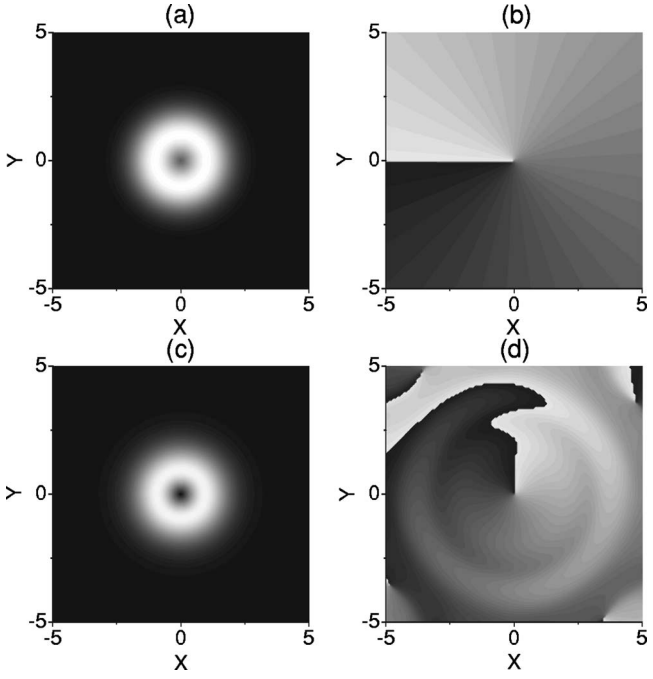

FIG. 4. Formation of a stable vortex with $S=1$ from a Gaussian input. (a),(b) The intensity and phase distributions in the initial Gaussian with a nested vortex. (c),(d) The intensity and phase distributions in the output ($t=700$). The input and output configurations have the norm, respectively, $N=6.406$ and $N=6.392$.

To further explore the robustness of the vortex which is predicted to be stable, in Fig. 4 we display its self-trapping from an arbitrarily chosen Gaussian input with a nested vortex, $u_0=Ar\exp(-\alpha r^2+i\theta)$, that has $A=1$ and $\alpha=1$. The shape of the input is far from the exact stable vortex soliton. In this case, we used a grid with 391×391 points and stepsizes $\Delta x=\Delta y=0.028$, $\Delta t=0.001$. Note that, at the values of N corresponding to the definitely stable solitons displayed in Figs. 3 and 4, a rather inaccurate stability condition proposed in Ref. [28] for the $S=1$ vortices would imply instability.

For the $S=1$ vortices which are predicted above to be unstable, we have found that, in the interval of

$$7.79 < N < 10.30, \tag{25}$$

which is adjacent to stability region (23) and occupies $\approx 1/8$ of the entire existence region of the vortices [cf. Eq. (24)],

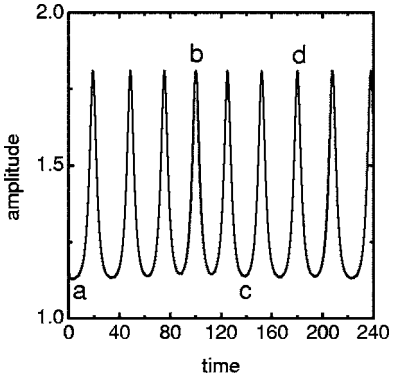

FIG. 5. Quasiperiodic evolution of the amplitude of the unstable $S=1$ vortex for $\mu=1.2$. The labels a, b, c, and d point at values of the amplitude at $t=0,100,140$, and 180 (see Fig. 6).

initial perturbations initiate *regular* quasiperiodic evolution, which features recurrent splittings of the soliton into two segments and their recombinations. The regular character of the evolution in this case is also manifest in nearly periodic oscillations of the soliton's amplitude, see typical examples in Figs. 5 and 6. This dynamical regime (which, to the best of our knowledge, has never been reported before) can be easily understood, as, unlike the known scenario of the instability development for vortex solitons in nonlinear-optical models in free space, where the splinters emerging after the breakup of the vortex soliton separate, moving away in tangential directions, in the present setting they cannot do it, being confined by the parabolic trap. We stress that Eq. (25) shows that the introduction of the vorticity makes it possible to *heighten* the actual collapse threshold for solitons in the trapped self-attractive condensate by a factor of 2: from $N_{\max}^{(S=0)}=5.85$ for the spinless solitons to $N\approx 11$ for their vortical counterparts.

For larger values of the norm, $10.3<N<N_{\max}^{(S=1)}\approx 24.1$, the evolution of the unstable vortex again starts with its splitting into two fragments; however, in this case they do not recombine, but rather quickly blow up (not shown here). The fact that the corresponding collapse threshold for the $S=1$ vortex solitons, found at $N=10.3$, is much smaller than the above-mentioned formal threshold, $N_{\max}^{(S=1)}\approx 24.1$, can be readily explained. Indeed, it has been shown above that the azimuthal instability sets in earlier than the radial instability that would directly lead to collapse. If the norm of each of

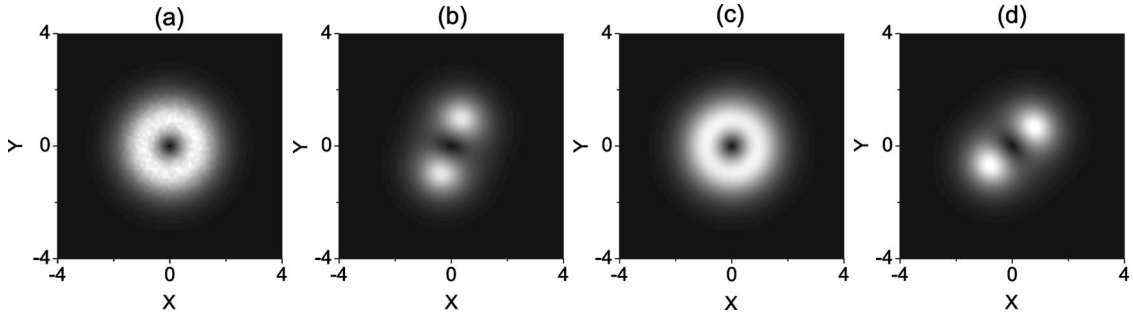

FIG. 6. Regular evolution of the unstable vortex with $S=1$ for $\mu=1.2$ initiated by random noise, which shows periodic splitting into two fragments and their subsequent recombination: (a) $t=0$, (b) $t=100$, (c) $t=140$, and (d) $t=180$. Here, values of the input and output norm are $N=8.476$ (at $t=0$) and $N=8.460$ (at $t=240$).

the zero-vorticity fragments, into which the vortex is broken by the azimuthal instability, is close enough to the collapse threshold for the $S=0$ solitons, i.e., $N_{\max}^{(S=0)}=5.85$, the fragments start collapsing and therefore fail to recombine into the vortex, unlike the situation with the weak instability in interval (25). This explanation is consistent with the fact that the actual collapse threshold for the vortex, $N=10.3$, is fairly close to $2N_{\max}^{(S=0)}$.

As concerns the $S=2$ solitons which were predicted above to be unstable at all finite values of N, the simulations (not shown here) demonstrate their irregular (chaotic) evolution for $0<N<10.4$. For $N>10.4$, they exhibit collapse, again through the splitting into a set of two $S=0$ solitons which then blow up intrinsically. Last, we have also checked that the zero-vorticity solitons in Eq. (8) exhibit collapse exactly when $N>N_{\max}^{(S=0)}=5.85$, as was assumed above.

At a late stage of the collapse, when the condensate will shrink to a size $\sim a_z$, the above derivation of the 2D equation (8) from its 3D counterpart (4) will break down, and the initially quasi-2D collapse will switch into a faster 3D blow-up mode. Direct simulations of the full 3D equation (11) corroborate this expectation, as will be reported in detail elsewhere.

V. VORTEX SOLITONS IN THE THREE-DIMENSIONAL GROSS-PITAEVSKII EQUATION

In this section, we aim to compare the above results, obtained in the framework of the 2D approximation, with what can be found from the full 3D equation (11), where the quasi-2D case corresponds to large Ω. Systematic presentation of the results for the 3D model will be a subject of a separate work, while here we report, in a brief form, findings which are most relevant for the comparison with the 2D approximation.

Stationary solutions for the 3D solitons with embedded vorticity S and chemical potential μ are looked for in the form [cf. Eq. (14)] $\Psi=R(r,z)\exp(iS\theta-i\mu t)$, where r,z,θ are cylindrical coordinates, and the real function R obeys the equation

$$\frac{\partial^2 R}{\partial r^2}+\frac{1}{r}\frac{\partial R}{\partial r}+\frac{\partial^2 R}{\partial z^2}+\left(2\mu-\frac{S^2}{r^2}-r^2-\Omega^2 z^2\right)R-2R^3=0, \tag{26}$$

supplemented by obvious boundary conditions: $R(r,z)\to 0$ when $r\to\infty$ or $|z|\to\infty$, and $R\sim r^S$ for $r\to 0$ at fixed z (we again define S to be $\geqslant 0$). After finding a family of the vortices from numerical solution of Eq. (26), their stability was investigated via the computation of eigenvalues for small perturbations.

First of all, the linear version of Eq. (26) can be considered similar to how it was done above for the 2D case: the solutions are built as linear combinations of products of the wave functions of the harmonic oscillator, cf. Eq. (16):

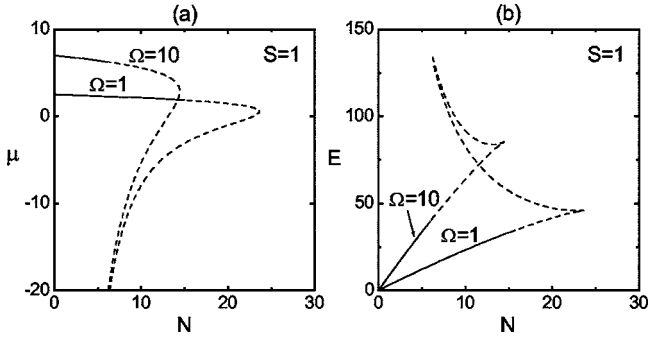

FIG. 7. The chemical potential (a) and energy (b) for families of three-dimensional solitons with the embedded vorticity $S=1$ vs the normalized number of atoms, with the moderately anisotropic ($\Omega=10$) and isotropic ($\Omega=1$) confining potentials. The continuous and dashed parts of the curves show, respectively, stable and unstable parts of the families.

$$\Psi_{jkl}(x,y,z,t)=e^{-i[j+k+1+(l+1/2)\Omega]t}\Phi_j(x)\Phi_k(y)\Phi_l(\sqrt{\Omega}z), \tag{27}$$

where $l=0,1,2,\ldots$ is the quantum number in the z direction. Being interested here in the "flattest" states (ones closest to the pancake configuration in the 3D space), we will set $l=0$. Then, wave functions with given vorticity S in the (x,y) plane are constructed as combinations of factorized wave functions (27), subject to the same constraint as in the 2D case, i.e., $j+k=S$. From this restriction and from the form of the chemical potential in the linear-limit solution (27) with $l=0$, $\mu=j+k+1+\Omega/2$, it follows that the chemical potential of solutions to the full nonlinear equation (26), obtained as a continuation starting from the linear limit, obeys a limitation

$$\mu<\mu_{\max}=S+1+\Omega/2, \tag{28}$$

cf. Eq. (20).

Numerically found families of the 3D soliton solutions with $S=1$ are characterized by $\mu(N)$ and $E(N)$ curves displayed in Fig. 7, one for the anisotropic model, with $\Omega=10$, and one for its isotropic counterpart, with $\Omega=1$. In the former case [which, as a matter of fact, is not a strongly anisotropic one, as the corresponding aspect ratio of the confinement lengths in the (x,y) and z directions is $\sqrt{10}$, pursuant to Eq. (1)], the existence and stability intervals of the fundamental vortices have been found to be, respectively, $0<N<14.46$, and

$$0<N<N_{\rm cr}^{(3D)}|_{\Omega=10}=5.95 \tag{29}$$

[cf. Eqs. (23) and (24) in the 2D model], hence the relative size of the stability area is ≈ 0.41. This should be compared to the relative size of the stability area in the 2D limit reported above, which is $\approx 1/3$. For the isotropic model ($\Omega=1$), the existence and stability intervals are, respectively, $0<N<23$, and

$$0<N<N_{\rm cr}^{(3D)}|_{\Omega=1}\approx 15, \tag{30}$$

their ratio being ≈ 0.65.

Thus, we conclude that the 2D limit yields a reasonable approximation for the pancake-shaped configurations (the

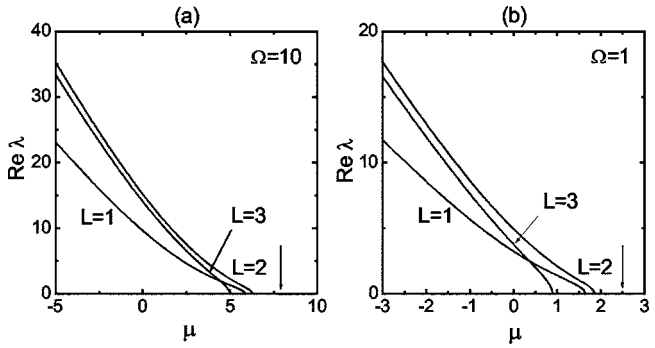

FIG. 8. The same as in Fig. 2(a), but for vortex solitons with $S=1$ in the full three-dimensional model: (a) $\Omega=10$; (b) $\Omega=1$. The arrows show the edge of the existence regions of the solitons on the scale of the chemical potential, as per Eq. (28).

relative difference between its prediction and the direct numerical result for the moderately anisotropic model with the aspect ratio $\sqrt{10}$ is $\simeq 20\%$). Another noteworthy conclusion is that the relative size of the stability area essentially increases as the 3D model approaches the isotropic configuration; in the isotropic limit, the relative size of the stability region is almost twice as large as in the 2D limit. In terms of the maximum value of the norm, $N_{\max}$, up to which the vortex soliton remains stable, the difference is still bigger: $N_{\max}$ for $\Omega=1$ exceeds its counterpart for $\Omega=10$ by a factor of ≈ 2.5.

To further illustrate the effect of the degree of asymmetry on the stability of vortex solitons, in Fig. 8 we display the spectrum of unstable eigenvalues for the 3D solitons with $S=1$, in the same two cases as considered above, i.e., the moderately anisotropic one with $\Omega=10$, and isotropic with $\Omega=1$. Comparison of this figure with the respective picture from Fig. 2(a) for the 2D model shows a gradual deformation of the spectrum with the transition from the 2D limit to the isotropic 3D configuration. An important observation is that the transition from the 2D approximation to the full 3D model does not lead to any new instability eigenmode (at least, up to the isotropic limit, $\Omega=1$); incidentally, the bending instability of the vortex core does not occur either.

As well as in the 2D case, vortex solitons with $S \geqslant 2$ [at least, the "flattest" ones, corresponding to $l=0$ in the linear limit, see Eq. (27)] are all unstable. As concerns the fundamental solitons with $S=0$, we could easily reproduce a known result stating that, as well as in the 2D model, they are stable within their full existence region, which is $N<3.8$ for $\Omega=10$, and $N<7.3$ for $\Omega=1$. Comparing these values with ones in Eqs. (29) and (30), we conclude that the introduction of the vorticity enhances the stability limit by a factor of 1.6 for $\Omega=10$, and by 2 for $\Omega=1$. Recall that, in the 2D model, the same enhancement factor was 1.3 [if its definition does not include the extra region (25) of the quasistable dynamical states]; this again demonstrates a general trend to the expansion of stability regions with the transition from the 2D limit to the fully isotropic 3D case.

VI. CONCLUSION

We have reported results of accurate investigation of the stability of localized vortices in Bose-Einstein condensates with self-attraction, trapped in the nearly two-dimensional configuration. We have briefly recapitulated the derivation of the effective 2D Gross-Pitaevskii equation from its full 3D counterpart, and demonstrated that, in the 2D limit, the vortices with $S=1$ are stable against azimuthal splitting in a *third* of their existence region, i.e., for $0<N<(1/3)N_{\max}^{(S=1)}$, in terms of the solution's norm (which is proportional to the number of atoms trapped in the vortex soliton). In the adjacent interval, $(1/3)N_{\max}^{(S=1)}<N<0.43N_{\max}^{(S=1)}$, the unstable vortex does not collapse, but rather demonstrates stable quasiperiodic dynamics, featuring cycles of splitting into two fragments and recombination, which is a quite interesting dynamical regime. For $N>0.43N_{\max}^{(S=1)}$, the two segments produced by the splitting fail to recombine, as they collapse intrinsically. The stable vortex soliton created in the pancake-shaped condensate of ^{7}Li may contain up to 10 000 atoms.

The results were checked against direct simulations of the 2D Gross-Pitaevskii equation, and, which is crucially important for the verification of their physical relevance, they were compared with the stability analysis of localized vortices in the full 3D equation. It was concluded that, for the moderately anisotropic 3D configuration with the aspect ratio $\sqrt{10}\approx 3.2$, the stability interval of the $S=1$ vortices occupies $\approx 40\%$ of their existence region (hence, the 2D limit provides for quite a reasonable approximation). In the 3D isotropic limit, the stability interval expands to 65% of the existence domain. The enhancement factor for the collapse threshold, caused by the introduction of vorticity $S=1$, was found too; in the 3D isotropic configuration it attains the value of 2. All higher-order localized vortices, with $S \geqslant 2$, are completely unstable, in the 2D limit and in the full 3D Gross-Pitaevskii equation alike.

ACKNOWLEDGMENTS

Support from Deutsche Forschungsgemeinschaft (DFG), Bonn, is acknowledged. The work of one of the authors (B.A.M.) was partially supported by the Israel Science Foundation through the Center-of-Excellence Grant No. 8006/03.

[1] M. R. Matthews, B. P. Anderson, P. C. Haljan, D. S. Hall, C. E. Wieman, and E. A. Cornell, Phys. Rev. Lett. **83**, 2498 (1999).

[2] P. Engels, I. Coddington, V. Schweikhard, and E. A. Cornell, J. Low Temp. Phys. **134**, 683 (2004).

[3] A. L. Fetter and A. A. Svidzinsky, J. Phys.: Condens. Matter **13**, R135 (2001).

[4] A. E. Leanhardt, A. Görlitz, A. P. Chikkatur, D. Kielpinski, Y. Shin, D. E. Pritchard, and W. Ketterle, Phys. Rev. Lett. **89**,

190403 (2002).
[5] L.-C. Crasovan, V. Vekslerchik, V. M. Pérez-García, J. P. Torres, D. Mihalache, and L. Torner, Phys. Rev. A **68**, 063609 (2003); Q. Zhou and H. Zhai, *ibid.* **70**, 043619 (2004); M. Möttönen, S. M. M. Virtanen, T. Isoshima, and M. M. Salomaa, *ibid.* **71**, 033626 (2005).
[6] L.-C. Crasovan, G. Molina-Terriza, J. P. Torres, L. Torner, V. M. Pérez-García, and D. Mihalache, Phys. Rev. E **66**, 036612 (2002).
[7] L.-C. Crasovan, V. M. Pérez-García, I. Danaila, D. Mihalache, and L. Torner, Phys. Rev. A **70**, 033605 (2004); N. S. Ginsberg, J. Brand, and L. V. Hau, Phys. Rev. Lett. **94**, 040403 (2005).
[8] G. A. Swartzlander and C. T. Law, Phys. Rev. Lett. **69**, 2503 (1992); A. W. Snyder, L. Poladian, and D. J. Mitchell, Opt. Lett. **17**, 789 (1992).
[9] I. Josopait, L. Dobrek, L. Santosa, A. Sanpera, and M. Lewenstein, Eur. Phys. J. D **22**, 85 (2003).
[10] C. C. Bradley, C. A. Sackett, J. J. Tollett, and R. G. Hulet, Phys. Rev. Lett. **75**, 1687 (1995).
[11] L. Khaykovich, F. Schreck, G. Ferrari, T. Bourdel, J. Cubizolles, L. D. Carr, Y. Castin, and C. Salomon, Science **296**, 1290 (2002); K. E. Strecker, G. B. Partridge, A. G. Truscott, and F. G. Hulet, Nature (London) **417**, 150 (2002).
[12] A. Görlitz, J. M. Vogels, A. E. Leanhardt, C. Raman, T. L. Gustavson, J. R. Abo-Shaeer, A. P. Chikkatur, S. Gupta, S. Inouye, T. Rosenband, and W. Ketterle, Phys. Rev. Lett. **87**, 130402 (2001).
[13] B. P. Anderson, P. C. Haljan, C. A. Regal, D. L. Feder, L. A. Collins, C. W. Clark, and E. A. Cornell, Phys. Rev. Lett. **86**, 2926 (2001).
[14] B. B. Baizakov, B. A. Malomed, and M. Salerno, Europhys. Lett. **63**, 642 (2003).
[15] J. Yang and Z. H. Musslimani, Opt. Lett. **28**, 2094 (2003).
[16] B. B. Baizakov, M. Salerno, and B. A. Malomed, in *Nonlinear Waves: Classical and Quantum Aspects*, edited by F. Kh. Abdullaev and V. V. Konotop (Kluwer Academic, Dordrecht, 2004), p. 61; also available at http://rsphy2.anu.edu.au/~asd124/Baizakov-2004-61-NonlinearWaves.pdf.
[17] H. Sakaguchi and B. A. Malomed, J. Phys. B **37**, 2225 (2004); E. A. Ostrovskaya and Y. S. Kivshar, Phys. Rev. Lett. **93**, 160405 (2004).
[18] B. B. Baizakov, B. A. Malomed, and M. Salerno, Phys. Rev. A **70**, 053613 (2004).
[19] D. Mihalache, D. Mazilu, F. Lederer, Y. V. Kartashov, L.-C. Crasovan, and L. Torner, Phys. Rev. E **70**, 055603(R) (2004).
[20] D. Mihalache, D. Mazilu, F. Lederer, B. A. Malomed, Y. V. Kartashov, L.-C. Crasovan, and L. Torner, Phys. Rev. Lett. **95**, 023902 (2005).
[21] D. Mihalache, D. Mazilu, F. Lederer, B. A. Malomed, L.-C. Crasovan, Y. V. Kartashov, and L. Torner, Phys. Rev. A **72**, 021601(R) (2005).
[22] B. A. Malomed, D. Mihalache, F. Wise, and L. Torner, J. Opt. B: Quantum Semiclassical Opt. **7**, R53 (2005).
[23] H. Saito and M. Ueda, Phys. Rev. Lett. **90**, 040403 (2003); F. Kh. Abdullaev, J. G. Caputo, R. A. Kraenkel, and B. A. Malomed, Phys. Rev. A **67**, 013605 (2003); G. D. Montesinos, V. M. Pérez-García, and H. Michinel, Phys. Rev. Lett. **92**, 133901 (2004); G. D. Montesinos, V. M. Pérez-García, and P. J. Torres, Physica D **191**, 193 (2004).
[24] P. G. Kevrekidis, G. Theocharis, D. J. Frantzeskakis, and B. A. Malomed, Phys. Rev. Lett. **90**, 230401 (2003).
[25] I. Towers and B. A. Malomed, J. Opt. Soc. Am. A **19**, 537 (2002).
[26] G. D. Montesinos, V. M. Pérez-García, H. Michinel, and J. R. Salgueiro, Phys. Rev. E **71**, 036624 (2005).
[27] F. Dalfovo and S. Stringari, Phys. Rev. A **53**, 2477 (1996); R. J. Dodd, J. Res. Natl. Inst. Stand. Technol. **101**, 545 (1996).
[28] T. J. Alexander and L. Bergé, Phys. Rev. E **65**, 026611 (2002).
[29] L. D. Carr and C. W. Clark, cond-mat/0408491.
[30] L. Bergé, Phys. Rep. **303**, 260 (1998).
[31] V. I. Yukalov and E. P. Yukalova, Phys. Rev. A **72**, 063611 (2005).
[32] V. I. Kruglov, V. M. Volkov, R. A. Vlasov, and V. V. Drits, J. Phys. A **21**, 4381 (1988); V. I. Kruglov, Yu. A. Logvin, and V. M. Volkov, J. Mod. Opt. **39**, 2277 (1992).
[33] W. J. Firth and D. V. Skryabin, Phys. Rev. Lett. **79**, 2450 (1997); L. Torner and D. V. Petrov, Electron. Lett. **33**, 608 (1997); D. Mihalache, D. Mazilu, L.-C. Crasovan, B. A. Malomed, and F. Lederer, Phys. Rev. E **61**, 7142 (2000).
[34] L.-C. Crasovan, B. A. Malomed, and D. Mihalache, Pramana, J. Phys. **57**, 1041 (2001); B. A. Malomed, G. D. Peng, P. L. Chu, I. Towers, A. V. Buryak, and R. A. Sammut, *ibid.* **57**, 1061 (2001).
[35] M. Quiroga-Teixeiro and H. Michinel, J. Opt. Soc. Am. B **14**, 2004 (1997); I. Towers, A. V. Buryak, R. A. Sammut, and B. A. Malomed, Phys. Rev. E, **63**, 055601(R) (2001); I. Towers, A. V. Buryak, R. A. Sammut, B. A. Malomed, L.-C. Crasovan, and D. Mihalache, Phys. Lett. A **288**, 292 (2001); B. A. Malomed, L.-C. Crasovan, and D. Mihalache, Physica D **161**, 187 (2002); D. Mihalache, D. Mazilu, L.-C. Crasovan, I. Towers, A. V. Buryak, B. A. Malomed, L. Torner, J. P. Torres, and F. Lederer, Phys. Rev. Lett. **88**, 073902 (2002); D. Mihalache, D. Mazilu, L.-C. Crasovan, I. Towers, B. A. Malomed, A. V. Buryak, L. Torner, and F. Lederer, Phys. Rev. E **66**, 016613 (2002); T. A. Davydova, and A. I. Yakimenko, J. Opt. A, Pure Appl. Opt. **6**, S197 (2004); D. Mihalache, D. Mazilu, B. A. Malomed, and F. Lederer, Phys. Rev. E **69**, 066614 (2004); H. Michinel, J. R. Salgueiro, and M. J. Paz-Alonso, *ibid.* **70**, 066605 (2004).
[36] D. Briedis, D. E. Petersen, D. Edmundson, W. Krolikowski, and O. Bang, Opt. Express **13**, 435 (2005); A. I. Yakimenko, Y. A. Zaliznyak, and Y. Kivshar, Phys. Rev. E **71**, 065603(R) (2005).
[37] Y. V. Kartashov, V. A. Vysloukh, and L. Torner, Phys. Rev. Lett. **94**, 043902 (2005).
[38] C. J. Pethick and H. Smith, *Bose-Einstein Condensation in Dilute Gases* (Cambridge University Press, Cambridge, 2002).
[39] D. S. Petrov, M. Holzmann, and G. V. Shlyapnikov, Phys. Rev. Lett. **84**, 2551 (2000); E. H. Lieb, R. Seiringer, and J. Yngvason, Commun. Math. Phys. **224**, 17 (2001); L. Salasnich, A. Parola, and L. Reatto, Phys. Rev. A **65**, 043614 (2002).
[40] S. Skupin, U. Peschel, L. Bergé, and F. Lederer, Phys. Rev. E **70**, 016614 (2004).
[41] J.-C. van der Meer, Nonlinearity **3**, 1041 (1990).
[42] R. L. Pego and H. A. Warchall, J. Nonlinear Sci. **12**, 347 (2002).
[43] N. N. Akhmediev, A. Ankiewicz, and H. T. Tran, J. Opt. Soc. Am. B **10**, 230 (1993).
[44] B. A. Malomed and R. S. Tasgal, Phys. Rev. E **49**, 5787

(1994); I. V. Barashenkov, D. E. Pelinovsky, and E. V. Zemlyanaya, Phys. Rev. Lett. **80**, 5117 (1998); A. De Rossi, C. Conti, and S. Trillo, *ibid.* **81**, 85 (1998); J. Schöllmann, R. Scheibenzuber, A. S. Kovalev, A. P. Mayer, and A. A. Maradudin, Phys. Rev. E **59**, 4618 (1999).

[45] D. Mihalache, D. Mazilu, and L. Torner, Phys. Rev. Lett. **81**, 4353 (1998); D. Mihalache, D. Mazilu, and L.-C. Crasovan, Phys. Rev. E **60**, 7504 (1999).

[46] J. M. Ortega and W. C. Rheinboldt, *Iterative Solution of Nonlinear Equations in Several Variables* (Academic, New York, 1970), p. 182.